AD-A130 930 ON THE MORPHOLOGY OF PLASMA DENSITY IRREGULARITIES IN 1/1
THE AURORAL F-REGION(U) SRI INTERNATIONAL MENLO PARK CA
J F VICKREY 01 APR 82 DNA-TR-81-79 DNA001-81-C-0076

UNCLASSIFIED F/G 20/9 NL

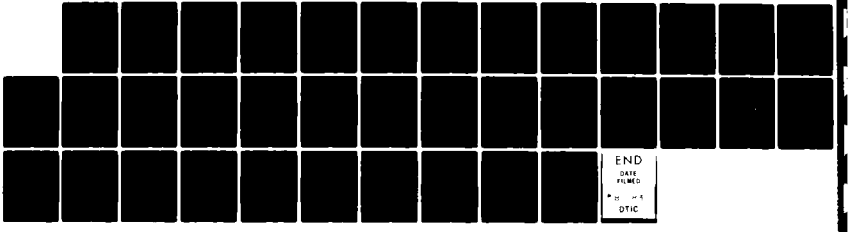

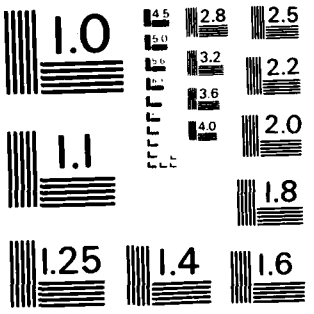

(12)

DNA-TR-81-79

ON THE MORPHOLOGY OF PLASMA DENSITY IRREGULARITIES IN THE AURORAL F- REGION

James F. Vickrey
SRI International
333 Ravenswood Avenue
Menlo Park, California 94025

1 April 1982

Technical Report

CONTRACT No. DNA 001-81-C-0076

THIS WORK WAS SPONSORED BY THE DEFENSE NUCLEAR AGENCY
UNDER RDT&E RMSS CODE B322081466 S99QAXHC00022 H2590D.

Prepared for
Director
DEFENSE NUCLEAR AGENCY
Washington, DC 20305

Destroy this report when it is no longer needed. Do not return to sender.

PLEASE NOTIFY THE DEFENSE NUCLEAR AGENCY, ATTN: STTI, WASHINGTON, D.C. 20305, IF YOUR ADDRESS IS INCORRECT, IF YOU WISH TO BE DELETED FROM THE DISTRIBUTION LIST, OR IF THE ADDRESSEE IS NO LONGER EMPLOYED BY YOUR ORGANIZATION.

UNCLASSIFIED

SECURITY CLASSIFICATION OF THIS PAGE (When Data Entered)

REPORT DOCUMENTATION PAGE		READ INSTRUCTIONS BEFORE COMPLETING FORM
1 REPORT NUMBER DNA-TR-81-79	2 GOVT ACCESSION NO. AD-A130 930	3 RECIPIENT'S CATALOG NUMBER
4 TITLE (and Subtitle) ON THE MORPHOLOGY OF PLASMA DENSITY IRREGULARITIES IN THE AURORAL F-REGION		5 TYPE OF REPORT & PERIOD COVERED Technical Report 6 PERFORMING ORG. REPORT NUMBER SRI Project 2623
7 AUTHOR(s) James F. Vickrey		8 CONTRACT OR GRANT NUMBER(s) DNA 001-81-C-0076
9 PERFORMING ORGANIZATION NAME AND ADDRESS SRI International 333 Ravenswood Avenue Menlo Park, California 94025		10 PROGRAM ELEMENT, PROJECT, TASK AREA & WORK UNIT NUMBERS Task S99QAXHC-00022
11 CONTROLLING OFFICE NAME AND ADDRESS Director Defense Nuclear Agency Washington, D.C. 20305		12 REPORT DATE 1 April 1982 13 NUMBER OF PAGES 36
14 MONITORING AGENCY NAME & ADDRESS(if different from Controlling Office)		15 SECURITY CLASS. (of this report) UNCLASSIFIED 15a DECLASSIFICATION DOWNGRADING SCHEDULE N/A since UNCLASSIFIED

16 DISTRIBUTION STATEMENT (of this Report)

Approved for public release; distribution unlimited.

17 DISTRIBUTION STATEMENT (of the abstract entered in Block 20, if different from Report)

18 SUPPLEMENTARY NOTES

This work was sponsored by the Defense Nuclear Agency under RDT&E RMSS Code B322081466 S99QAXHC00022 H2590D.

19 KEY WORDS (Continue on reverse side if necessary and identify by block number)

Plasma Density Irregularities
High Latitudes
Propagation Disturbance
Auroral Zone

20 ABSTRACT (Continue on reverse side if necessary and identify by block number)

In this report a framework for understanding the morphology of high latitude plasma density irregularities is developed that has three component parts. Namely, to predict irregularity morphology one must specify (1) the source of irregularities, (2) the lifetimes of irregularities once produced, and (3) the redistribution of irregularities by magnetospheric convection. An irregularity morphology model is developed using the simplest possible source function, classical diffusion, and a simple two-celled magnetospheric

DD FORM 1 JAN 73 1473 EDITION OF 1 NOV 65 IS OBSOLETE

UNCLASSIFIED

SECURITY CLASSIFICATION OF THIS PAGE (When Data Entered)

20. ABSTRACT (Continued)

convection model. While the qualitative results of this model are encouraging, emphasis is placed on its limitations and how it can be improved in the future. The motivation for this study is two-fold; first, it is important to predict the severity of propagation disturbances in the nuclear disturbed environment. In the absence of actual nuclear data, naturally occurring auroral disturbances provide a test bed for assessing the accuracy of predictive codes. Second, naturally occurring plasma density irregularities hinder DoD communications and surveillance systems. Therefore, understanding the processes that control the evolution and ultimate morphology of naturally structured plasma can help to predict system performance and perhaps develop mitigants.

TABLE OF CONTENTS

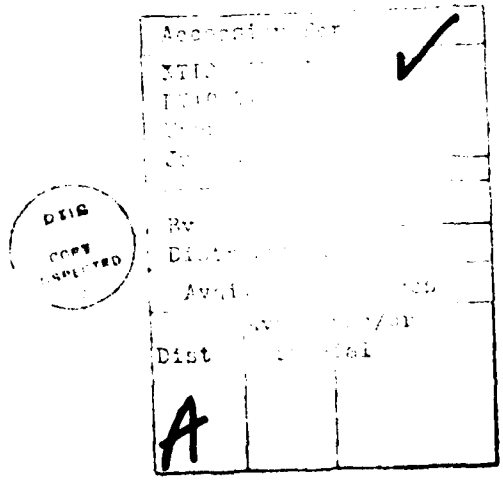

LIST OF ILLUSTRATIONS

I INTRODUCTION

The Earth's F-region ionospheric plasma displays structure perpendicular to the magnetic field on scales from hundreds of kilometers down to centimeters. The physical processes that operate over such a wide range of scale sizes are, of course, very diverse. At the largest scales ($\lambda \gtrsim 10$ km), production, loss, and transport of structured plasma are dominated by aeronomic processes including energy sources of magnetospheric origin. At intermediate (0.1 km $< \lambda <$ 10 km) and small ($\lambda <$ 100 m) scales, plasma instabilities and cross-field plasma diffusion are often the dominant physical processes controlling the plasma structure. However, because nonlinear plasma processes can couple strcutures in one scale length regime to other spatial frequencies, the entire spectrum of irregularities must be studied as a whole.

Polar orbiting satellites find two main zones of maximum irregularity occurrence in the F-layer ionosphere, as detected by both plasma density and electric field fluctuation sensors. One is located near the nighttime magnetic equator. The other zone is located throughout the vast high-latitude region bounded roughly by the polar cusp in the local time zone 0800-1400 and by the equatorial boundary of the high-latitude convection pattern at other local times. This equatorward boundary for the polar zone of structure is thus well equatorward of the classical auroral oval at most local times.

In both of these irregularity zones, the structured plasma can disrupt transionospheric radio wave communication channels. Hence, the interest is practical as well as purely scientific in understanding the processes that control the production, evolution, and decay of plasma structure. The equatorial zone has received the most attention in the recent past in both the theoretical and experimental arenas. This is in part due to the relatively large data base available from radar and rocket measurements made under DNA support at the equator.

However, the aeronomic processes are simpler and the sources of free energy capable of driving the F-region plasma dynamics are fewer at the equator than at high latitudes. For example, at mid- and low-latitudes, F-region dynamics are governed principally by neutral atmospheric winds and waves and the dynamo electric field; at high latitudes, these processes are accompanied by particle precipitation, magnetospheric convection electric fields, and auroral current systems flowing parallel and perpendicular to the magnetic field. Nevertheless, the considerable progress made recently in defining and understanding the key physical processes that structure plasma at the equator can also be beneficial to high-latitude studies because many of the processes occurring there (particularly the plasma instabilities) are analogous.

In the next section, we briefly summarize the present understanding of high-latitude plasma structuring phenomena and present a set of working hypotheses that form a framework for investigating the origin and spatial extent of high-latitude irregularities. In the concluding section, we point out the areas for future study that may have the greatest impact on improving this framework. Emphasis is placed on the important contributions that the new DNA polar orbiting satellite, Sondrestrom Radar, and EISCAT may yield.

II MECHANISMS RESPONSIBLE FOR THE OBSERVED MORPHOLOGY OF F-REGION PLASMA STRUCTURE AT HIGH LATITUDES

To predict the observed F-region plasma structure on a global basis, there are three fundamental questions that must be answered:

(1) When and where are plasma density irregularities produced?

(2) How long do they last?

(3) How far do they convect during their lifetime?

A. Irregularity Production

Perhaps the most obvious source of structured plasma at high latitudes is the structured particle precipitation responsible for the aurora. Using satellite data, Dyson and Winningham [1974] showed a one-to-one correlation between the 300 eV electron flux boundary and the penetration of an irregular plasma region. The spatial and temporal structure of incoming precipitation has not yet been examined in sufficient detail (particularly at the low particle energies that produce F-layer ionization) to definitively assess the direct contribution of the spatial spectrum of precipitation to that of the resulting ionization. However, during one rocket flight from Greenland the outer scale of precipitation and plasma density were observed in-situ simultaneously to be $\sim$ 50 km, a value that is similar to that observed in the F-layer ionization enhancements, as measured by incoherent-scatter radar [Kelley et al., 1982]. This agreement suggests that structured soft-particle precipitation is a major source of large-scale F-region plasma density irregularities.

An example of large-scale F-layer density structure, as measured by the Chatanika incoherent-scatter radar, is illustrated in Figure 1, which shows contours of constant electron density as a function of altitude and invariant latitude. The data are displayed in a coordinate

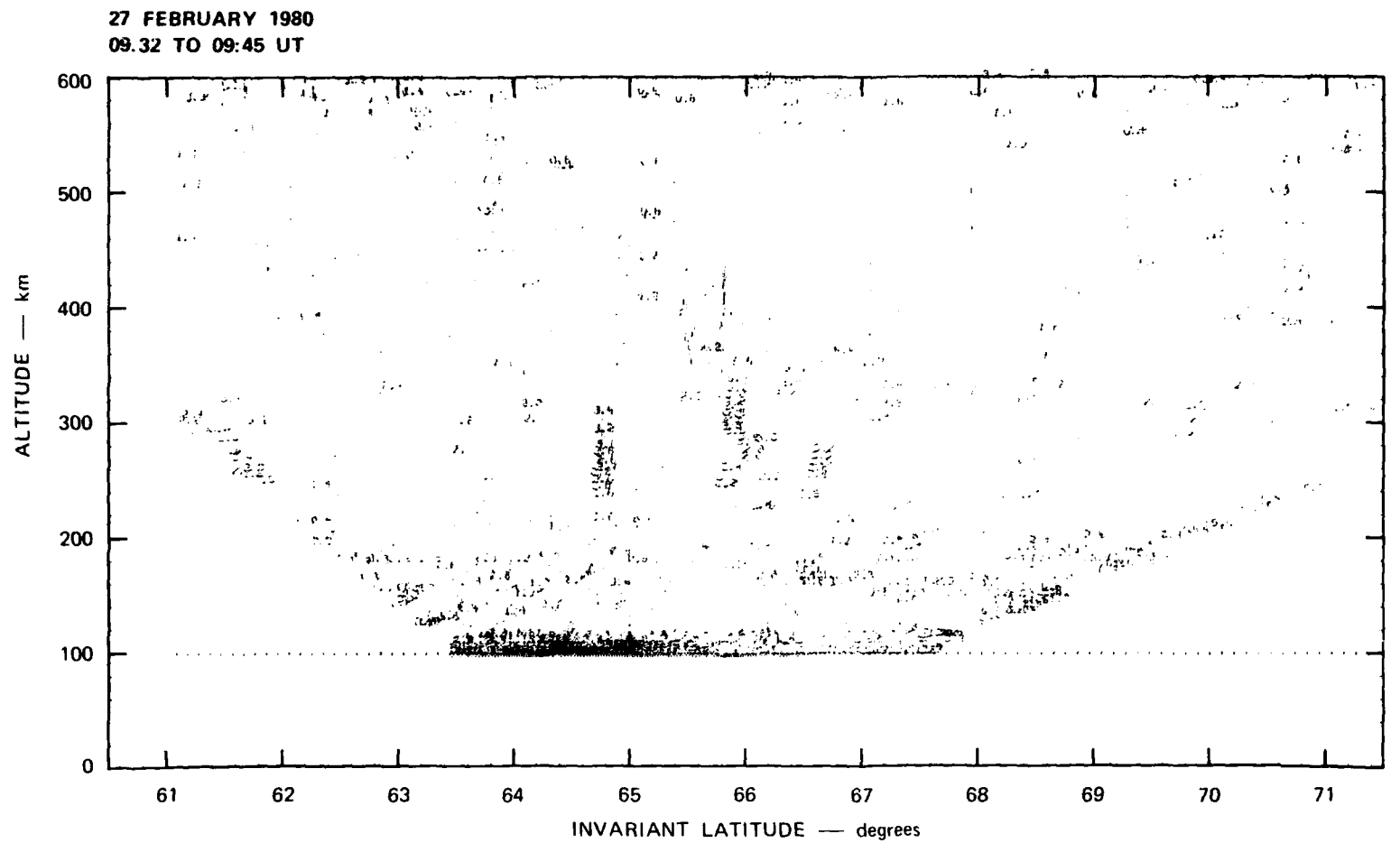

FIGURE 1 ALTITUDE/LATITUDE VARIATION OF ELECTRON DENSITY IN THE MIDNIGHT-SECTOR AURORAL ZONE MEASURED BY THE CHATANIKA RADAR

system with straight, vertical magnetic field lines. These observations from the midnight vector (LT = UT - 10 hours) show F-region ionization enhancements or plasma "blobs" that reach $\sim$ 5-6 $\times$ 10^5 cm^{-3}, which is approximately an enhancement by a factor of five over the background. Plasma-density enhancements ranging from a factor of two to ten over the background are very commonplace at Chatanika. These blobs are often observed to convect into the radar field of view from the north (i.e., following the usual midnight-sector convection pattern) and their appearance is not necessarily associated with magnetic activity [Vickrey at al., 1980].

These plasma blobs can be considered analogous to equatorial "bubbles" because they provide large-scale density gradients upon which convective plasma instabilities can operate to produce intermediate- and small-scale plasma structures. Indeed, the steep blob edges are unstable to the gradient drift instability [Linson and Workman, 1970] on one side or the other, depending on the local configuration of electric field and neutral wind. Ossakow and Chaturvedi [1979] have pointed out that field-aligned currents, which are known to be a permanent feature of the high latitude ionosphere, are also a destabilizing factor. Vickrey et al. [1980] combined measurements from the Chatanika radar and TRIAD satellite to show that the large-scale plasma blobs are linearly unstable to a generalized form of the $\bar{E} \times \bar{B}$ instability that includes the effects of field-aligned currents. They also verified the existence of intermediate-scale plasma structure ($\lambda \approx 1$ km) associated with the blobs by detecting scintillation enhancements on the TRIAD 150-MHz telemetry signal. Other evidence for "edge"-related plasma instabilities comes from a rocket flight across an auroral arc [Kelley and Carlson, 1977; Kelley et al., 1975]. At the edge of the arc intense (10 mV/m) oxygen ion cyclogron waves were observed as were broadband short wavelength electrostatic emissions with $k_\perp \rho_i \approx 1$, where ρ_i is the ion gyro radius. Field-aligned currents, perpendicular plasma shear flow, and parallel sheared-electron flow [Keskinen, private communication, 1982] have all been invoked to explain these waves. Above the arc itself, the F layer was smooth at these smaller scales.

An important difference between the operation of convective instabilities at the nighttime equatorial ionosphere and at high latitudes is the presence of a highly conducting, precipitating-particle-produced E layer in the auroral zone to which the F-region irregularities are connected via the geomagnetic field. E-region "shorting" reduces the growth rate of the convective instabilities and, as will be discussed more fully below, reduces the lifetime of F-layer irregularities for scale sizes large enough to map to the E layer [i.e., $\lambda \gtrsim 1$ km; Vickrey and Kelley (1982)]. However, the presence of the E layer may make it possible to tap the magnetospheric energy source that might otherwise not be available.

An additional source of structured plasma density at high latitudes is the structure in the magnetospheric convection electric field. This structuring of plasma density can come about in two principal ways. First, where the electric field is large, there can be a large velocity difference between ions and neutrals as well as an increase in ion temperature over the neutral gas temperature because of enhanced Joule heating. Both of these effects increase the recombination rate of O^+ with N_2 and result in a change of ion composition of O^+ to NO^+. Because the NO^+ recombination rate is relatively large, a density depletion can occur wherever the electric field is enhanced (i.e., $E \gtrsim 40$ mV/m). Such effects have been observed at Chatanika [Kelly and Wickwar, 1981]. Although we expect this process to be important only at large scales, detailed studies of the magnitude of electric field gradients have not been performed to date.

Second, structured electric fields can produce structured density by simply mixing flux tubes that have varying plasma density [Fejer and Kelley, 1980]. A turbulent magnetospheric electric field acting on a horizontal density gradient can thus produce much the same result as a local convective instability. Extreme examples of such turbulent fields are often observed in the winter polar cap during periods of extended B_z north conditions. (An Example from OGO-6 [Heppner, 1977] is shown in Figure 2.) No study has been conducted to date, however, regarding the size of velocity shears normally observed in the lower ionosphere and

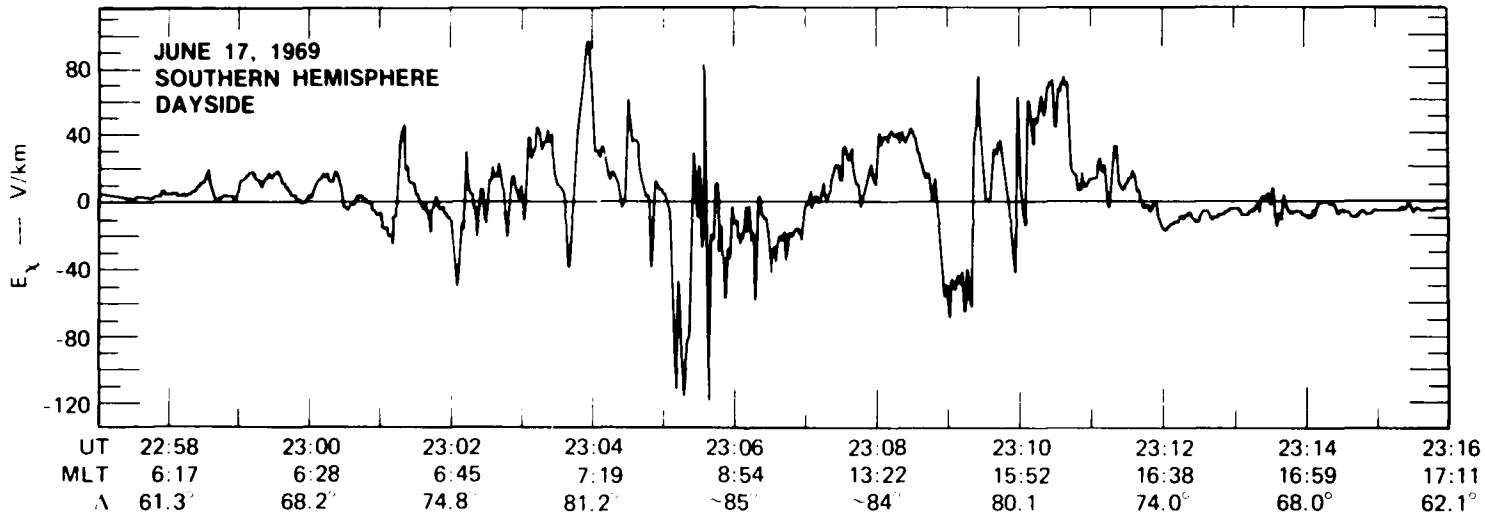

FIGURE 2 AN EXAMPLE OF HIGHLY IRREGULAR ELECTRIC FIELDS IN THE DAYSIDE WINTER HEMISPHERE

at what scale sizes they might stir plasma of varying density. Kintner [1976] found shear frequencies (dV/dx) the order of 10^{-1} to 10^{-2} Hz in the upper ionosphere ($\sim$ 2000-km altitude). Mozer et al. [1979] have pointed out that electrostatic shocks are imbedded in regions of intense turbulent electric fields. However, how these map to the F layer is not clear because of the strong evidence for collocated parallel electric fields. Kelley and Carlson [1977] found a shear frequency of 20 Hz in an arc-boundary crossing, but that may be an extreme case.

B. Irregularity Lifetime

The second element in our framework for understanding the morphology of structured plasma at high latitudes is irregularity lifetime. Because we are considering plasma structure in the F layer, recombination will reduce the absolute density on adjacent flux tubes equally (for small amplitude irregularities) and hence, will not reduce horizontal density structure. Thus, the major process governing the removal of F-region plasma density irregularities, once they are produced, is cross-magnetic-field plasma diffusion. A possibly important process that is ignored in the present discussion is the damping of irregularities by convection into a region in which (or a temporal variation resulting in which) the electric field and neutral wind configuration is stabilizing.

The plasma density gradient at the edge of an irregularity has an associated pressure gradient that tends to cause the plasma to diffuse away from regions of more dense plasma and into areas of less dense plasma. The diffusion rate, d_j ($= \rho_j \nu_j$ where ρ_j is the Larmor radius and ν_j is the collision frequency for species j), is larger for ions than for electrons in the F layer because their gyro radius and, hence, their horizontal displacement per collision is much larger than for electrons (even though their collision frequency with neutrals is less than the electron ion collision frequency). However, when the ions try to diffuse away from the electrons, an electrostatic field is produced, which retards ion diffusion. The net result is that the plasma, as a whole, diffuses at twice the slow electron rate.

Let us now consider the effects of a highly conducting auroral E-region, to which the F-layer irregularities may be electrically connected. The electrons in the F layer can easily move along the magnetic field to the E region. In the E region, they participate in horizontal current systems to short out the ambipolar electrostatic field that would otherwise retard ion diffusion. Thus, for a highly conducting E region, classical diffusion proceeds at the ion (rather than the electron) rate. Because ions carry the cross field current and electrons the parallel current, an "image" forms in the E region and acts to slow the net diffusion. However, recombination prevents this for a scale-size λ if $n \gtrsim 10^4/\lambda^2$, where λ is in km and n is cm^{-3} [Vickrey and Kelley, 1982].

Vickrey and Kelley [1982] have constructed a simple model of classical cross-field plasma diffusion in the F region including E-region conductivity effects. They have found that the cross-field diffusion rate depends strongly on the height of the E and F layers as well as their peak electron densities. The fundamental quantity governing the diffusion rate, however, is the ratio of Pedersen conductivities in the E and F regions, Σ_p^E/Σ_p^F. Figure 3 shows the cross-field diffusion rate, $D_\perp$, and lifetime, $\tau_{1\ km}$, of one-kilometer-scale irregularities [$\tau_\lambda = (\lambda^2/4\pi^2 D_\perp)$] as a function of Σ_p^E/Σ_p^F for typical F-region parameters. The presence of a highly conducting E region can enhance the F-region cross-field plasma diffusion rate by an order of magnitude.

C. High-Latitude Convection

The final element necessary to explain high-latitude irregularity morphology is convection. Large-scale unstable blobs of plasma such as that shown in Figure 1 are observed to convect with the background electric field [Vickrey et al., 1980]. These large-scale features have very long lifetimes and, thus, can convect far from their origins. Plasma instabilities operating on their edges may produce small-scale plasma structure all along the way. This "cascade" to small scale reduces the lifetime of the large-scale features, but not enough to prevent their transit across the polar cap [Kelley et al., 1982]. This

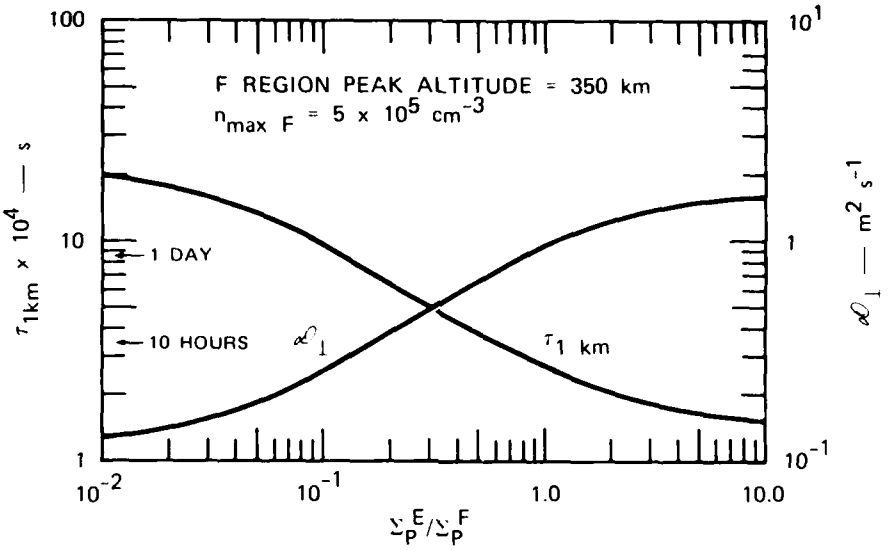

FIGURE 3 THE DEPENDENCE OF CROSS-FIELD DIFFUSION RATE, $D_\perp$, AND LIFETIME OF ONE-km-SCALE IRREGULARITIES, $\tau_{1\ km}$, ON THE RATIO OF E- TO F-REGION PEDERSEN CONDUCTIVITIES

scenario can explain the presence of plasma structure throughout the polar regions of the earth even though "source" regions may be quite localized.

As a framework it is useful to see to what extent a classical aeronomic viewpoint can explain the data. To this end Kelley et al. [1982] have quantified a classical picture of irregularity formation and distribution by combining simple models of irregularity production and loss with a two-celled magnetospheric convection pattern. They considered a simple "source" region of irregularities to be an annular ring near the poleward edge of the auroral oval. This source is a region in which satellites have recorded soft precipitating particle fluxes [Foster and Burrows, 1976; Hardy, private communication]. The irregularity lifetime was calculated using the classical diffusion model of Vickrey and Kelley [1982], which includes E-region conductivity effects. The global E-region conductivity distribution assumed was that given by Spiro et al., [1978]. Figure 4 shows the results obtained by Kelley et al., [1982]. The trajectories (in the inertial frame) of four flux tubes across the polar cap and around the auroral zone are shown. The numbers indicate the amplitude in dB of one-kilometer-scale irregularities, $|\Delta N/N|^2$, where N is electron density. The amplitude is

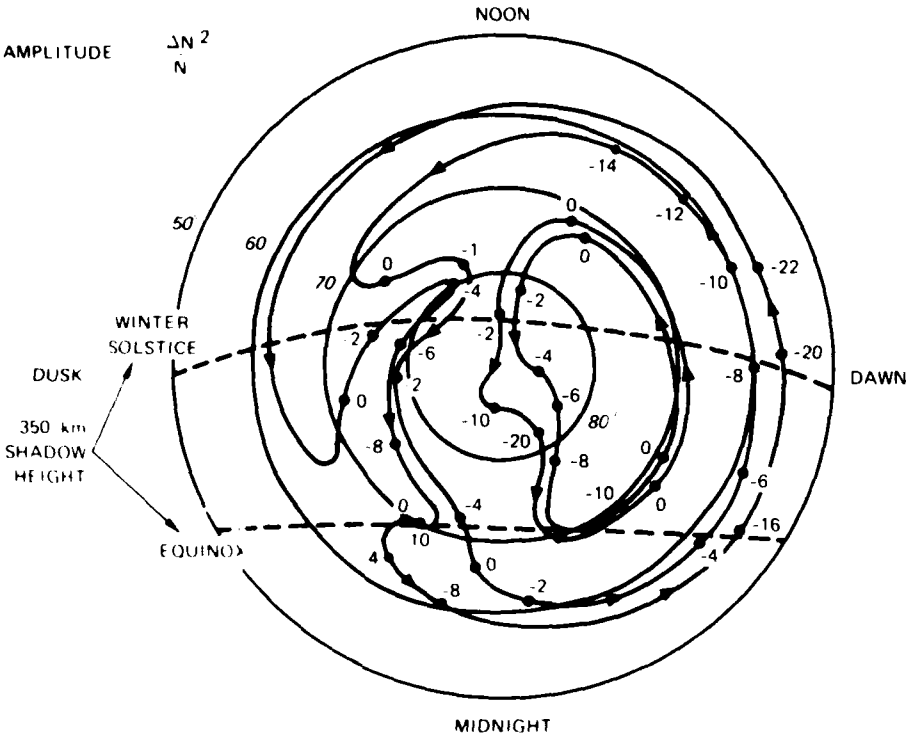

FIGURE 4 ILLUSTRATION OF THE LATITUDE AND LOCAL-TIME VARIATIONS (IN THE INERTIAL FRAME) OF THE AMPLITUDE (IN dB) OF ONE-km-SCALE ELECTRON DENSITY IRREGULARITIES

reset to 0 dB whenever the trajectories cross the source region near the poleward edge of the auroral oval. A similar plot for 10-km structures would show almost negligible decay, because diffusion acts 100 times more slowly at that scale size.

Figure 5 is a similar plot that includes the overall decay of the ionosphere because of recombination, which reduces the irregularity and background density by approximately 4 dB per hour of travel time. This plot, then, is more representative of the spectral strength $|\Delta N|^2$; hence, it is perhaps more descriptive of scintillation effects. The peak F-region density is assumed 5×10^5 cm^{-3} in the production zone, with the density maximum at a height of 350 km. A Chapman layer is also assumed [Vickrey and Kelley, 1982]. Winter conditions are taken

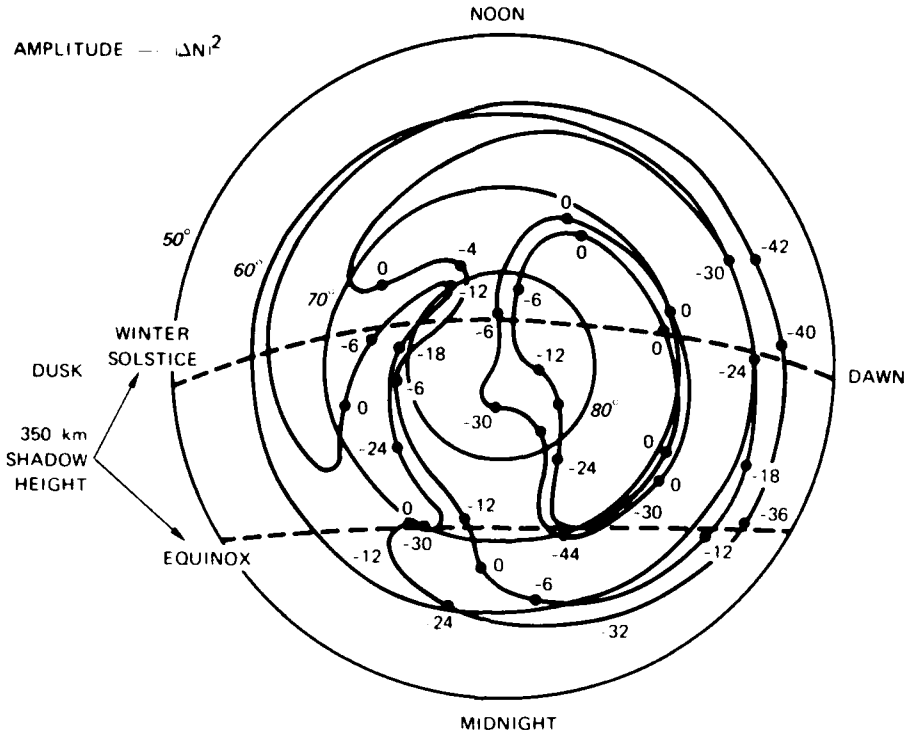

FIGURE 5 ILLUSTRATION OF THE LATITUDE AND LOCAL-TIME VARIATIONS (IN THE INERTIAL FRAME) OF THE AMPLITUDE (IN dB) OF ONE-km-SCALE ELECTRON DENSITY IRREGULARITIES INCLUDING THE EFFECTS OF RECOMBINATIONAL DECAY

so as to emphasize the effects of auroral production and decay. A dashed line marks the terminator at 350-km altitude during winter and equinox. When the absolute density decayed to 5×10^3 cm^{-3}, the recombination decay was stopped. In such a case, the assumption of an O^+ plasma is no longer valid, and longer-lived ions may dominate the F_2 layer composition [Heelis et al., 1981].

Despite the simplicity of this first attempt to assess the relative roles of production, convection, and decay in determining high-latitude irregularity morphology, this model leads to a number of useful conclusions. For example, 10-km size density fluctuations can survive transport throughout the polar cap and auroral zone if sunlight does not illuminate

the region for a prolonged period and fill in the background. At one-kilometer scale, the classical diffusion discussed here and in Vickrey and Kelley [1982] has a significant effect in some regions of the polar cap and auroral zone. For example, a very deep irregularity "hole" can be formed in the central polar cap, as experimentally reported by Kelley and Mozer [1972]. This is primarily due to the long time that a flux tube can spend in the central polar region. Even in the 10-km case, a very sharp gradient in irregularity intensity is formed at the equatorward edge of the nighttime magnetospheric-convection zone--not the auroral oval. This agrees excellently with many studies of the high-latitude irregularity boundary [see review by Fejer and Kelley, 1980]. However, other sources of plasma density irregularities, such as mid-latitude spread F and processes associated with plasma density gradients near the F-region trough can also contribute to irregularity formation at times.

In relatively quiet times, the postsunset local-time region, 1800 to 2100, between 60° and 68° should not contain many irregularities because, in the nonrotating frame, flux tubes only enter this region from the sunlit sector. For the same reason, the equatorward boundary of the irregularity zone should be at higher latitudes in the dusk sector than in the dawn sector, to which midnight-sector auroral-oval irregularities can rapidly convect. This agrees with the ISIS results reported by Sagalyn et al., [1974], who showed that the boundary was about 3° higher in latitude in the dusk sector for $K_p \leq 3$. The difference was less pronounced for $K_p > 3$. This is reasonable because, with increasing magnetic activity, large convection speeds can dominate over the corotation velocity at lower latitudes in the local time sector near and just after dusk.

Note that, although the source function would be much different from that used to construct Figure 5, the high density debris from a nuclear exchange would at late times eventually be transported and distributed in accordance with this flow pattern. The extremely long lifetimes expected for the structured plasma could, thus, impact on DoD communications and surveillance systems at great distances from, and for long periods after a detonation.

We turn now to ways in which the classical model does not fit the observations. Figure 6 shows the average electric field strength at 31 Hz (~ 200-m scale fluctuations) measured by the OV1-17 satellite [Kelley and Mozer, 1972] as a function of invariant latitude. Note that the irregularity amplitude has a latitudinal trend that is qualitatively similar to that expected from Figures 4 and 5 in a noon-to-midnight cross section. Namely, there is a strong source of irregularities in the polar cusp, a decay of irregularity amplitude in the central polar cap, and another source region in the midnight-sector auroral oval. These observations make it apparent, however, that the simple model illustrated in Figures 4 and 5 grossly misrepresents the amplitude of small-scale irregularities; for example, the decrease in amplitude for 200-m scales in Figures 4 and 5 should be multiplied by a factor of 25. However, the amplitude decrease actually observed across the polar cap for 200-m scales is even less than that expected for kilometer-scale structures. These data thus suggest that intermediate-

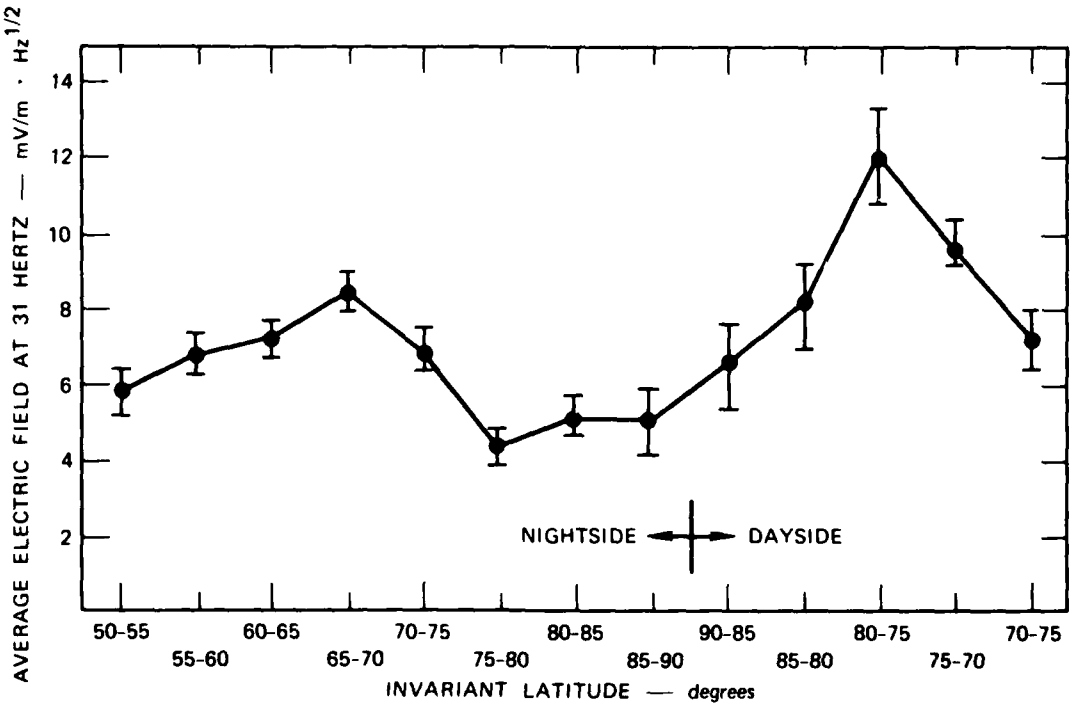

FIGURE 6 AVERAGE ELECTRIC-FIELD STRENGTH AT 200-m SCALE AS A FUNCTION OF LATITUDE

and small-scale irregularities are continuously generated throughout the polar cap, probably on the unstable edges of the larger-scale blobs. As mentioned above, such a cascade process would hasten the removal of large-scale features, but not enough to prevent their transit through the polar cap.

It is interesting to turn the problem around by interpreting Figure 6 in terms of anomalous diffusion at large scales. This can be done as follows: Suppose the irregularity spectrum $S(k) = |\Delta N(k)|^2$, has a rigid shape (e.g., $S(k) \propto k^{-2}$) as a set of adjacent flux tubes convect across the polar cap. Then, the decrease in amplitude of 200-m irregularities reflects a decrease in energy stored at the input scale, which is of order $\lambda \approx 10$ km. The quasi-exponential spatial decrease in irregularity amplitude in Figure 6 between 75° invariant latitude on the dayside cusp and 75° on the nightside can be converted to an effective diffusion rate, D_{eff}, if we assume the average antisunward drifts from the Spiro et al. [1978] convection model. This exercise leads to an effective diffusion rate that is within ~ 60 percent of the Bohm diffusion rate measured empirically in laboratory plasmas. This D_{eff} is approximately 100 times faster than the classical diffusion rate.

The above calculation is obviously too approximate and based on too many unverified assumptions to prove conclusively that the Bohm diffusion process is operating in the polar cap. Nonetheless, it strongly suggests that some anomalous process is operating that is much faster than classical diffusion. To proceed in the future, it will be necessary to measure the complete spectrum of irregularities and their associated electric fields across the polar regions to distinguish between anomalous diffusion processes due to various microinstabilities [e.g., Gary, 1980]. This will be discussed more fully in Section III.

D. Irregularity Geometry

Any viable theory for the formation and evolution of plasma structure must ultimately account for the observed geometry of plasma density irregularities. Auroral-zone scintillation measurements from

the Wideband satellite show enhancements in scintillation whenever the propagation vector lies in the plane of the local L-shell, not just when it coincides with the local magnetic field line. This phenomenon suggests that the intermediate-scale ($\sim$ 1 km) irregularities responsible for the scintillation are L-shell-aligned sheet-like structures rather than simple rods. This unexpected geometry has been confirmed by spaced-receiver scintillation measurements in the midnight sector auroral zone. These measurements show a high ratio (up to 10 to 1) of spatial coherence in the magnetic east-west direction as compared to the north-south direction [Rino et al., 1978]. The linear gradient drift and current convective instabilities operating on the meridional density gradients shown in Figure 1 tend to produce irregularities with a $\hat{k}$ vector in the east-west plane; i.e., orthogonal to the geometry of the kilometer-scale structures that is actually observed. This apparent paradox has been addressed by Chaturvedi and Ossakow [1972a, b], whose analysis shows that the linearly unstable mode of the gradient drift and current convective instabilities can transfer energy through nonlinear coupling to a (linearly stable) mode whose wave vector lies in the plane of the density gradient.

Recently, Keskinen and Ossakow [1982] have performed numerical simulations of the gradient drift and current convective instabilities operating on a blob such as shown in Figure 1 for typical auroral F-region conditions. They have found that the primary and associated (secondary) small-scale structures can be oriented in either the north-south or east-west direction depending on the ambient electric field magnitude and direction. Because the meridional electric-field component in the auroral zone is typically five times the zonal component, any primary (north-south) structure can be quickly destabilized by the meridional electric-field component to produce secondary structure, which is east-west aligned.

Another mechanism for producing kilometer-scale east-west structures in the auroral zone can result if the large-scale blobs themselves are not infinitely extended in the east-west direction. Any large-scale zonal gradients can be acted upon by the meridional

electric field to produce (primary) east-west aligned structure. Recently, a campaign of experiments with the Chatanika radar was conducted to measure east-west structure of the large-scale blobs. The preliminary results from those experiments indicate that although the east-west scale lengths can be very much longer than those north-south (particularly during magnetically quiet times), there are also occasions when the east-west extent of the blobs is comparable to the meridional extent (Tsunoda, private communication).

Another process that might explain the observed anisotropy of medium-scale irregularities at high latitudes is the behavior of an incompressible fluid in a sheared convective-flow pattern. A very simple example is illustrated schematically in Figure 7. The situation was constructed to be similar to the premidnight sector convective flow pattern out of the polar cap, where flow is principally sun-aligned, and into the auroral oval, where flow is principally zonal. An irregularity represented by the ellipsoid contour of constant electron density was chosen to be initially sun aligned (i.e., perpendicular to what is

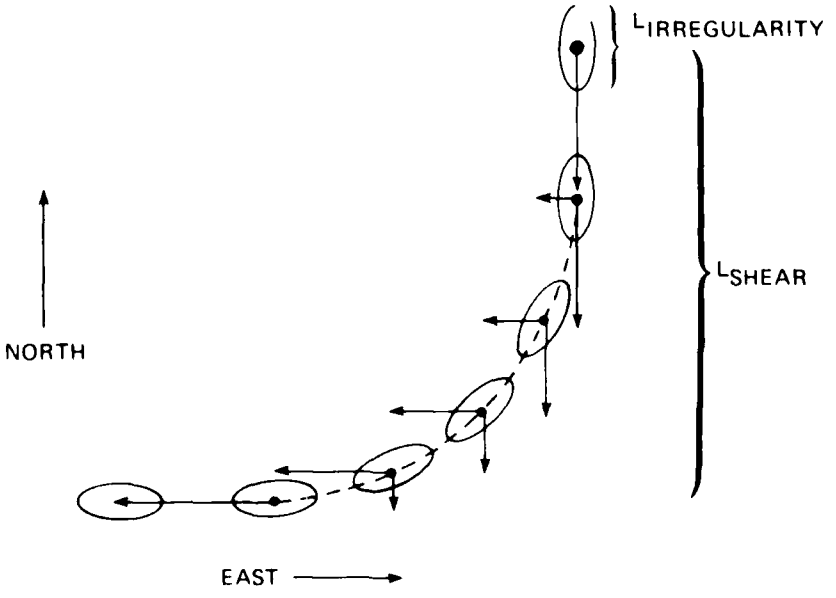

FIGURE 7 SCHEMATIC ILLUSTRATION OF AN ANISOTROPIC IRREGULARITY SUBJECTED TO A SHEARED FLOW PATTERN

observed in the auroral zone). Because the F region plasma is incompressible, the area of the ellipsoid remains constant. The equatorward tip of the irregularity enters the region of westward flow before the poleward tip. Therefore, the irregularity becomes either kinked or smoothly rotated (depending on the ratio of irregularity size, $L_{irregularity}$, to shear (or rotation) size, L_{shear}) as it drifts further south. In general, however, we expect the irregularity to be aligned with the streamlines of flow. Thus this model predicts east-west aligned sheets in the auroral oval except perhaps very near the Harang discontinuity. It is interesting to note that a conservative velocity shear (given by assuming that a 500 m/s meridional flow in the polar cap changes to a 500 m/s westward flow in the auroral oval over a meridional distance of 500 km) is on the order of 10^{-3} Hz. This value is comparable to the $\overline{E} \times \overline{B}$ instability growth rates observed by Vickrey et al. [1980] for an unstable blob. Thus, by the time an irregularity has formed, it should already be rotated to align with flow lines.

Evidence that convection may indeed influence irregularity geometry can be found in the latitude-local time variations of anisotropy determined from spaced receiver scintillation measurements. Figure 8 shows the preliminary results of such a compilation (R. C. Livingston, private communication) for Wideband Satellite passes recorded at Poker Flat, Alaska (65° invariant latitude, Local Time = UT - 10 hours) during February and March of 1978. The data show a dramatic change in kilometer scale irregularity anisotropy between the polar cap where irregularities appear to be isotropic or rod-like depending on local time and lower latitudes where irregularities can be sheet-like throughout the evening. Note that the elongation of the sheets and rods is reduced in the midnight sector (i.e., near the Harang discontinuity). One possible reason why the polar cap irregularities appear to be isotropic or rod-like may be that the winter polar cap flow is very irregular. A similar analysis of summer polar cap data (where flow is expected to be more regular) is underway.

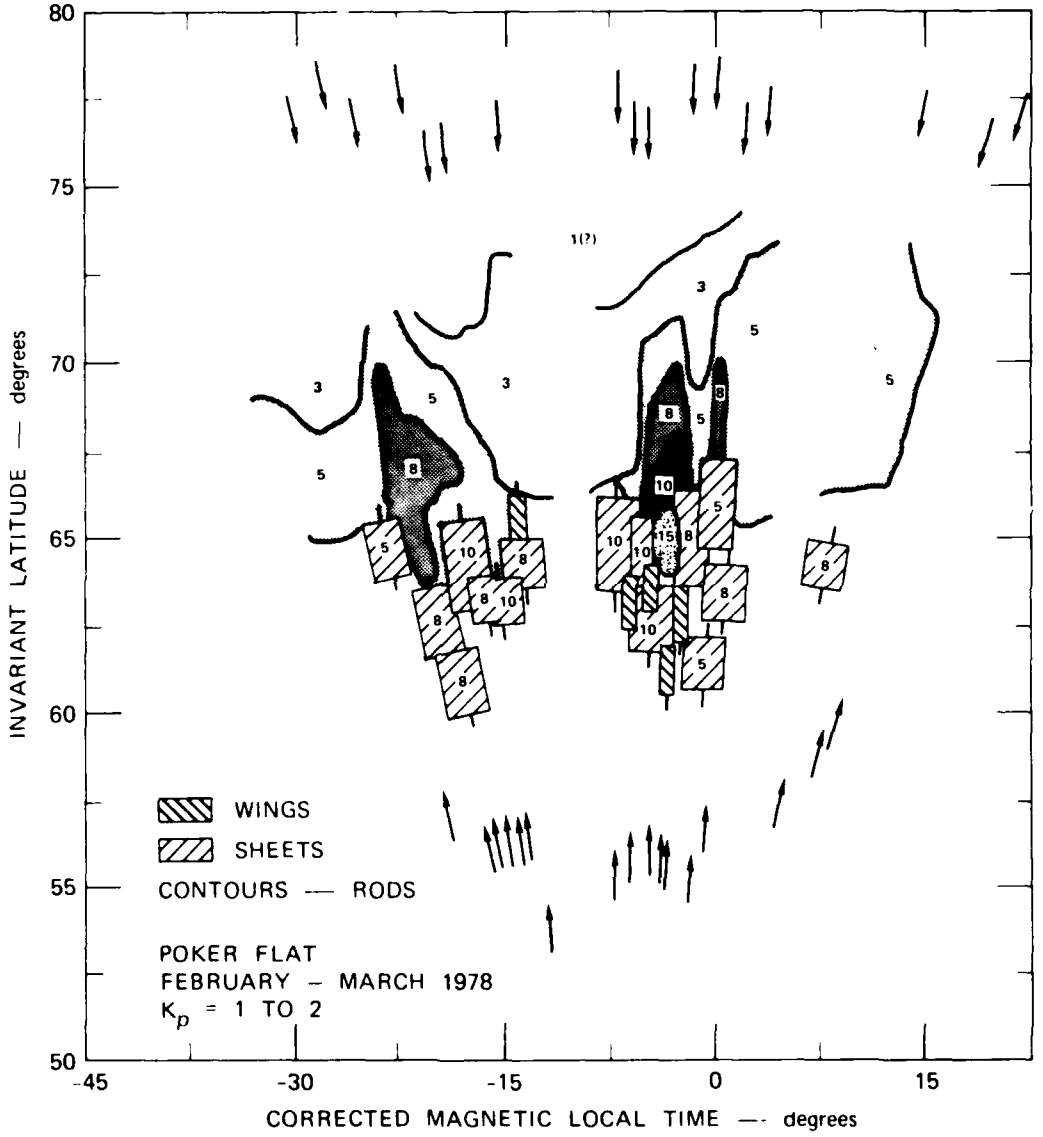

FIGURE 8 LATITUDE-LOCAL-TIME VARIATION OF IRREGULARITY ANISOTROPY

III FUTURE RESEARCH

Our framework for understanding high-latitude irregularity morphology consists of three simple component parts--irregularity production, transport, and decay. It is clear, however, that none of these component parts is well understood at present. Indeed, fundamental questions remain in each area that can be addressed by the new DNA satellite, the Sondrestrom Radar, and EISCAT.

In the area of irregularity production, the source regions of large-scale blobs are known to be much more complicated than the simple ring used in the model of Kelley et al. [1982]. For example, sun-aligned F layer polar cap arcs are known to be a strong source of radio wave scintillation [Weber and Buchau, 1980] and thus should be included in the "source function." This large-scale source function can be better defined by analyzing data from precipitating-particle detectors aboard polar-orbiting satellites and perhaps from satellite imaging. These measurements should be augmented by ground-based incoherent-scatter measurements that can probe the three-dimensional density structure that results from this precipitation. It is important that the particle detector have a high spatial resolution because at present the nature of the spatial spectrum of soft precipitation is unknown. For example, can structured precipitation directly produce structured ionization at kilometer scales and smaller or is precipitation only responsible for large-scale "seed" features upon which instabilities operate? Because the E-region conductivity produced by energetic precipitation is an important consideration for both the growth rate of convective instabilities and for the lifetime of irregularities once they are produced, the particle detector should also be sensitive to high energies so that the global conductivity pattern can be modeled.

It has been shown that convective plasma instabilities are operative in the high-latitude ionosphere. However, they have many important properties that merit further examination. For example, it is now becoming clear that the spectrum of irregularities present on a given flux tube of plasma depends in a complicated way on the past history of that flux tube. Thermal diffusion operates slowly as compared to observed instability growth rates. Thus, instability growth is, to some extent, cumulative as a flux tube convects between unstable and benign regions. Therefore, to predict the amount of plasma structure at a given point, the minimum destabilizing influences a flux tube has encountered in crossing the polar regions must be assessed. These influences include the magnitude and direction of the electric field and neutral wind with respect to the density gradient as well as the amplitude of the field-aligned current, which is known to be a permanent feature of the auroral zone. Measurement of the latter can be performed by a satellite-borne vector magnetometer; however, detailed knowledge of the neutral wind pattern at high-latitudes requires more extensive ground-based optical measurements as well as improved modeling. Simultaneous in-situ measurement of δE and $\delta n/n$ should help separate the various instability mechanisms. This has been used successfully at the magnetic equator to identify drift waves as an important contributor to the cascade of energy from long to short scales [Kelley et al., 1982].

High-latitude convection can be measured by polar orbiting satellites with electric-field detectors as well as by incoherent-scatter radar. It is important to further characterize the global changes in this pattern caused by variations in the interplanetary magnetic field and solar wind conditions. Moreover, high spatial-resolution electric-field measurements are required to determine the magnitude of velocity shears. Furthermore, small-scale waves that are thought to play a role in anomalous diffusion (which may in turn be the controlling factor determining irregularity lifetime) can be detected and studied. For example, in the equatorial case, it has been shown that waves of the drift-mode type are more easily detected

through their electric-field signatures and that the wave type can be identified through comparisons of δE and $\delta n/n$ [Kelley et al., 1982]. Other crucial elements in the study of anomalous diffusion are to measure the entire spectrum of density structure from hundreds of kilometers to meters, if possible, and to document spectral changes between the polar cap, auroral zone, and trough.

The complicated geometry of plasma density irregularities is an interesting area for further research. Whether this geometry is the result of precipitation structure, nonlinear saturation of a convective instability, a secondary instability, or simply a result of convective flow patterns is an open question. Certainly the answer will depend upon the scale size of interest. At large scales, combined ground-based optical and incoherent-scatter radar measurements may shed some light on the answer. At intermediate and small scales, further spaced-receiver scintillation measurements are required.

REFERENCES

Chaturvedi, P. K., and Ossakow, S. L., "Nonlinear Stabilization of the E × B Gradient Drift Instability in Ionospheric Plasma Clouds," J. Geophys. Res., Vol. 84, No. A2, p. 419 (February 1979).

Chaturvedi, P. K., and Ossakow, S. L., "Nonlinear Stabilization of the Current Convective Instability in the Diffuse Aurora," J. Geophys. Letts., Vol. 6, No. 12, p. 957 (December 1979).

Dyson, P. L., and Winningham, J. D., "Topside Ionospheric Spread F and Particle Precipitation in the Dayside Magnetospheric Clefts," J. Geophys. Res., Vol. 79, p. 5219 (1974).

Fejer, B. G., and Kelley, M. C., "Ionospheric Irregularities," Rev. Geophys. and Space Sci., Vol. 18, No. 2, p. 401 (May 1980).

Foster, J. C. and Burrows, J. R., "Electron Fluxes Over the Polar Cap: 1. Intense KeV Fluxes During Post-Storm Quieting," J. Geophys. Res., Vol. 81, No. 34, p. 6016 (December 1976).

Gary, S. P., "Wave Particle Transport From Electrostatic Instabilities," Phys. Fluids, Vol. 23, No. 6, p. 1193 (June 1980).

Heelis, R. A., Murphy, J. A., and Hanson, W. B., "A Feature of the Behavior of He^+ in the Nightside High-Latitude Ionosphere During Equinox," J. Geophys. Res., Vol. 86, No. A1, p. 59 (January 1981).

Heppner, J. P., "Empirical Models of High-Latitude Electric Fields," J. Geophys. Res., Vol. 82, No. 7, p. 1115 (March 1977).

Kelley, M. C., and Carlson, C. W., "Observation of Intense Velocity Shear and Associated Electrostatic Waves Near an Auroral Arc," J. Geophys. Res., Vol. 82, p. 2343 (1977).

Kelley, M. C., and Mozer, F. S., "A Satellite Survey of Vector Electric Fields in the Ionosphere at Frequencies of 10-500 Hz: 1. Isotropic, High-Latitude Electrostatic Emissions," J. Geophys. Res., Vol. 77, No. 22, p. 4158 (August 1972).

Kelley, M. C., Bering, C. E., and Mozer, F. S., "Evidence That the Ion Cyclotron Instability is Saturated by Ion Heating," Phys. Fluids, Vol. 18, p. 1590 (1975).

Kelley, M. C., Vickrey, J. F., Carlson, C. W., and Torbert, R., "On the Origin and Spatial Extent of High-Latitude F-region Irregularities," J. Geophys. Res., in press.

Kelley, M. C., Pfaff, C. R., Baker, K. D., Ulwick, J. C., Livingston, R. C., Rino, C. L., and Tsunoda, R. T., "Simultaneous Rocket Probe and Radar Measurements of Equatorial Spread F--Transitional and Short Wavelength Results," submitted to J. Geophys. Res.

Kelly, J. D., and Wickwar, V. B., "Radar Measurements of High-Latitude Ion Composition Between 140 and 300-km Altitude," J. Geophys. Res., Vol. 86, No. A9, p. 7617 (September 1981).

Keskinen, M. J., and Ossakow, S. L., "Nonlinear Evolution of Plasma Enhancements in the Auroral Ionosphere: 1. Long Wavelength Irregularities," J. Geophys. Res., Vol. 87, p. 144 (January 1982).

Kintner, P. M., "Observations of Velocity Shear Driven Plasma Turbulence," J. Geophys. Res., Vol. 81, p. 5114 (1976).

Linson, L. M. and Workman, J. B, "Formation of Striations in Ionospheric Plasma Clouds," J. Geophys. Res., Vol. 75, No. 16, p. 3211 (June 1970).

Mozer, F. S., Cattell, C. A., Temerin, M., Torbert, R. B., Vonglinski, S., Woldorf, M., and Wygant, J., "The dc and ac Electric Field, Plasma Density, Plasma Temperature, and Field-Aligned Current Experiments on the S3-3 Satellite," J. Geophys. Res., Vol. 84, No. A10, p. 5875 (1979).

Ossakow, S. L., and Chaturvedi, P. K., "Current Convective Instability in the Diffuse Aurora," Geophys. Res. Letts., Vol. 6, No. 4, p. 322 (April 1979).

Rino, C. L., Livingston, R. C., and Matthews, S. J., "Evidence for Sheet-Like Auroral Ionospheric Irregularities," Geophys. Res. Letts., Vol. 5, No. 12, p. 1034 (December 1978).

Sagalyn, R. S., Smiddy, M., and Ahmed, M., "High-Latitude Irregularities in the Topside Ionosphere Based on ISIS 1 Thermal Probe," J. Geophys. Res., Vol. 79, No. 28, p. 4253 (October 1974).

Spiro, R. W., Heelis, R. A., and Hanson, W. B., "Ion Convection and the Formation of the Mid-Latitude F-region Ionization Trough," J. Geophys. Res., Vol. 82, No. A9, p. 4255 (September 1978).

Vickrey, J. F., and Kelley, M. C., "The Effects of a Conducting E layer on Classical F-region Cross-Field Plasma Diffusion," submitted to J. Geophys. Res.

Vickrey, J. F., Rino, C. L., and Poterma, T. A., "Chatanika/Triad Observations of Unstable Ionization Enhancements in the Auroral F region," Geophys. Res. Letts., Vol. 7, No. 10, p. 789 (October 1980).

Wallis, D. D., and Budzinski, E. E., "Empirical Models of Height-Integrated Conductivities," J. Geophys. Res., Vol. 86, No. A1, p. 125 (January 1981).

Weber, E. J., and Buchau, J., "Polar Cap F-layer Auroras," Geophys. Res. Letts., Vol. 8, No. 1, p. 125 (January 1980).

DISTRIBUTION LIST

DEPARTMENT OF DEFENSE

Assistant to the Secretary of Defense
Atomic Energy
ATTN: Executive Assistant

Command & Control Technical Center
ATTN: C-650
ATTN: C-312, R. Mason
ATTN: C-650, G. Jones
3 cy ATTN: C-650, W. Heidig

Defense Communications Agency
ATTN: Code 230
ATTN: Code 205
ATTN: J300 for Yen-Sun Fu

Defense Communications Engineer Center
ATTN: Code R410, N. Jones
ATTN: Code R410
ATTN: Code R410, R. Craighill
ATTN: Code R123

Defense Intelligence Agency
ATTN: DB-4C, E. O'Farrell
ATTN: DC-7B
ATTN: DB, A. Wise
ATTN: DT-1B
ATTN: DIR

Defense Nuclear Agency
ATTN: STNA
ATTN: NAFD
ATTN: RAEE
ATTN: NATD
ATTN: RAAE, P. Lunn
3 cy ATTN: RAAE
4 cy ATTN: TITL

Defense Technical Information Center
12 cy ATTN: DD

Dep Under Secretary of Defense
Comm, Cmd, Cont & Intell
ATTN: Dir of Intelligence Sys

Field Command
Det 1, Defense Nuclear Agency
Lawrence Livermore Lab
ATTN: FC-1

Field Command
Defense Nuclear Agency
ATTN: FCPR
ATTN: FCTXE
ATTN: FCTT, G. Ganong
ATTN: FCTT, W. Summa

Interservice Nuclear Weapons School
ATTN: TTV

Joint Chiefs of Staff
ATTN: C3S
ATTN: C3S, Evaluation Office (HDOO)

DEPARTMENT OF DEFENSE (Continued)

Joint Strat Tgt Planning Staff
ATTN: JLA, Threat Applications Div
ATTN: JLTW-2

National Security Agency
ATTN: W-32, O. Bartlett
ATTN: R-52, J. Skillman
ATTN: B-3, F. Leonard

Under Secy of Def for Rsch & Engrg
ATTN: Strategic & Space Sys (OS)
ATTN: Strat & Theater Nuc Forces, B. Stephan

WWMCCS System Engineering Org
ATTN: J. Hoff

DEPARTMENT OF THE ARMY

Assistant Chief of Staff for Automation & Comm
ATTN: DAMO-C4, P. Kenny

Atmospheric Sciences Laboratory
ATTN: DELAS-EO, F. Niles

BMD Advanced Technology Center
ATTN: ATC-R, D. Russ
ATTN: ATC-O, W. Davies
ATTN: ATC-R, W. Dickinson
ATTN: ATC-T, M. Capps

BMD Systems Command
ATTN: BMDSC-HLE, R. Webb
2 cy ATTN: BMDSC-HW

Deputy Chief of Staff for Ops & Plans
ATTN: DAMO-RQC, C2 Div

Harry Diamond Laboratories
ATTN: DELHD-NW-P
ATTN: DELHD-NW-R, R. Williams

US Army Chemical School
ATTN: ATZN-CM-CS

US Army Comm-Elec Engrg Instal Agency
ATTN: CCC-EMEO-PED, G. Lane
ATTN: CCC-CED-CCO, W. Neuendorf

US Army Communications Command
ATTN: CC-OPS-W
ATTN: CC-OPS-WR, H. Wilson

US Army Communications R&D Command
ATTN: DRDCO-COM-RY, W. Kesselman

US Army Foreign Science & Tech Ctr
ATTN: DRXST-SD

US Army Materiel Dev & Readiness Cmd
ATTN: DRCLDC, J. Bender

DEPARTMENT OF THE ARMY (Continued)

US Army Nuclear & Chemical Agency
ATTN: Library

US Army Satellite Comm Agency
ATTN: Document Control

US Army TRADOC Sys Analysis Actvy
ATTN: ATAA-PL
ATTN: ATAA-TCC, F. Payan, Jr
ATTN: ATAA-TDC

USA Missile Command
ATTN: DRSMI-YSO, J. Gamble

DEPARTMENT OF THE NAVY

Joint Cruise Missiles Project Ofc
ATTN: JCMG-707

Naval Air Systems Command
ATTN: PMA 271

Naval Electronic Systems Command
ATTN: PME 117-211, B. Kruger
ATTN: PME 106-13, T. Griffin
ATTN: Code 501A
ATTN: PME 117-20
ATTN: PME 117-2013, G. Burnhart
ATTN: Code 3101, T. Hughes
ATTN: PME 106-4, S. Kearney

Naval Intelligence Support Ctr
ATTN: NISC-50

Naval Ocean Systems Center
ATTN: Code 5322, M. Paulson
ATTN: Code 532
ATTN: Code 5323, J. Ferguson

Naval Research Laboratory
ATTN: Code 4720, J. Davis
ATTN: Code 4780
ATTN: Code 7500, B. Wald
ATTN: Code 4780, S. Ossakow
ATTN: Code 6700
ATTN: Code 7950, J. Goodman
ATTN: Code 4187
ATTN: Code 4700

Naval Space Surveillance System
ATTN: J. Burton

Naval Surface Weapons Center
ATTN: Code F31

Naval Telecommunications Command
ATTN: Code 341

Ofc of the Deputy Chief of Naval Ops
ATTN: OP 981N
ATTN: OP 941D
ATTN: NOP 654, Strat Eval & Anal Br

Office of Naval Research
ATTN: Code 412, W. Condell
ATTN: Code 414, G. Joiner

DEPARTMENT OF THE NAVY (Continued)

Strategic Systems Project Office
ATTN: NSP-2141
ATTN: NSP-2722, F. Wimberly
ATTN: NSP-43

Theater Nuclear Warfare Prj Office
ATTN: PM-23, D. Smith

DEPARTMENT OF THE AIR FORCE

Aerospace Defense Command
ATTN: DC, T. Long

Air Force Geophysics Laboratory
ATTN: OPR, H. Gardiner
ATTN: OPR-1
ATTN: LKB, K. Champion
ATTN: CA, A. Stair
ATTN: PHY, J. Buchau
ATTN: R. Babcock
ATTN: R. O'Neil

Air Force Technical Applications Ctr
ATTN: TN

Air Force Weapons Laboratory
ATTN: SUL
ATTN: NTYC
ATTN: NTN

Air Force Wright Aeronautical Lab
ATTN: A. Johnson
ATTN: W. Hunt

Air Logistics Command
ATTN: OO-ALC/MM

Air University Library
ATTN: AUL-LSE

Assistant Chief of Staff
Studies & Analyses
ATTN: AF SASC, C. Rightmeyer
ATTN: AF SASC, W. Kraus

Ballistic Missile Office
ATTN: ENSN, W. Wilson
ATTN: SYC, Col Kwan

Deputy Chief of Staff
Research, Development, & Acq
ATTN: AFRDS, Space Sys & C3 Dir
ATTN: AFRDSS
ATTN: AFRDSP

Deputy Chief of Staff
Operations and Plans
ATTN: AFXOCD
ATTN: AFXOAT
ATTN: AFXOKS

Electronic Systems Div
ATTN: [illegible] Clark

Electronic Systems Division
ATTN: [illegible]

DEPARTMENT OF THE AIR FORCE (Continued)

Electronic Systems Division
ATTN: SCS-1E
ATTN: SCS-2, Lt Col Vinkels

Foreign Technology Division
ATTN: NIIS Library
ATTN: TQTD, B. Ballard

Rome Air Development Center
ATTN: OCS, V. Coyne
ATTN: TSLD

Rome Air Development Center
ATTN: EEP, J. Rasmussen

Space Division
ATTN: YGJB, W. Mercer
ATTN: YKM, Maj Alexander
ATTN: YKM, Cpt Norton

Stragetic Air Command
ATTN: NRT
ATTN: DCX
ATTN: XPFS
ATTN: ADWATE, B. Bauer
ATTN: DCXT, T. Jorgensen

OTHER GOVERNMENT AGENCIES

Central Intelligence Agency
ATTN: OSWR/SSD for K. Feuerpfetl
ATTN: OSWR/NED

Department of Commerce
National Bureau of Standards
ATTN: Sec Ofc for R. Moore

Department of Commerce
National Oceanic & Atmospheric Admin
ATTN: R. Grubb

Institute for Telecommunications Sciences
ATTN: L. Berry
ATTN: A. Jean
ATTN: W. Utlaut

NATO

NATO School (SHAPE)
ATTN: US Documents Officer

DEPARTMENT OF ENERGY CONTRACTORS

EG&G, Inc
ATTN: D. Wright
ATTN: J. Colvin

University of California
Lawrence Livermore National Lab
ATTN: Technical Info Dept Library
ATTN: L-389, R. Ott
ATTN: L-31, R. Hager

Sandia National Labs, Livermore
ATTN: T. Cook
ATTN: B. Murphey

DEPARTMENT OF ENERGY CONTRACTORS (Continued)

Los Alamos National Laboratory
ATTN: MS 664, J. Zinn
ATTN: P. Keaton
ATTN: D. Simons
ATTN: MS 670/J. Hopkins
ATTN: T. Kunkle, ESS-5
ATTN: R. Jeffries
ATTN: J. Wolcott
ATTN: C. Westervelt

Sandia National Lab
ATTN: D. Dahlgren
ATTN: Tech Lib 3141
ATTN: Space Project Div
ATTN: D. Thornbrough
ATTN: Org 1250, W. Brown
ATTN: Org 4231, T. Wright

DEPARTMENT OF DEFENSE CONTRACTORS

Aerospace Corp
ATTN: V. Josephson
ATTN: T. Salmi
ATTN: R. Slaughter
ATTN: I. Garfunkel
ATTN: J. Straus
ATTN: D. Olsen

Analytical Systems Engineering Corp
ATTN: Radio Sciences

Analytical Systems Engineering Corp
ATTN: Security

BDM Corp
ATTN: L. Jacobs
ATTN: T. Neighbors

Berkeley Research Associates, Inc
ATTN: J. Workman
ATTN: S. Brecht
ATTN: C. Prettie

Boeing Aerospace Co
ATTN: MS 87-63, D. Clauson

Boeing Co
ATTN: S. Hall
ATTN: S. Tashird

Booz-Allen & Hamilton, Inc
ATTN: B. Wilkinson

BR Communications
ATTN: J. McLaughlin

University of California at San Diego
ATTN: H. Booker

Charles Stark Draper Lab, Inc
ATTN: A. Tetewski
ATTN: J. Gilmore
ATTN: D. Cox

Computer Sciences Corp
ATTN: F. Eisenbarth

DEPARTMENT OF DEFENSE CONTRACTORS (Continued)

Comsat Labs
ATTN: D. Fang
ATTN: G. Hyde

Cornell University
ATTN: D. Farley, Jr
ATTN: M. Kelly

E-Systems, Inc
ATTN: R. Berezdivin

Electrospace Systems, Inc
ATTN: H. Logston
ATTN: P. Phillips

EOS Technologies, Inc
ATTN: B. Gabbard

ESL, Inc
ATTN: R. Ibaraki
ATTN: R. Heckman
ATTN: J. Lehman
ATTN: E. Tsui
ATTN: J. Marshall

General Electric Co
ATTN: C. Zierdt
ATTN: A. Steinmayer

General Electric Co
ATTN: G. Millman

General Research Corp
ATTN: B. Bennett

GEO-Centers, Inc
ATTN: E. Marram

Harris Corp
ATTN: E. Knick

Honeywell, Inc
ATTN: G. Collyer, Avionics Dept
ATTN: G. Terry, Avionics Dept

Horizons Technology, Inc
ATTN: R. Krujer

HSS, Inc
ATTN: D. Hamser

IBM Corp
ATTN: M. Slander

Institute for Defense Analyses
ATTN: E. Bauer
ATTN: H. Wolfhard
ATTN: J. Aein
ATTN: M. Bates

International Tel & Telegraph Corp
ATTN: Technical Library

International Tel & Telegraph Corp
ATTN: G. Wetmore

JAYCOR
ATTN: J. Sperling

DEPARTMENT OF DEFENSE CONTRACTORS (Continued)

JAYCOR
ATTN: J. Doncarlos

Johns Hopkins University
ATTN: J. Newland
ATTN: T. Evans
ATTN: P. Komiske
ATTN: J. Phillips

Kaman Sciences Corp
ATTN: T. Stephens

Kaman Tempo
ATTN: B. Gambill
ATTN: DASIAC
ATTN: J. Devore
ATTN: W. Knapp
ATTN: K. Schwartz
ATTN: W. McNamara

Litton Systems, Inc
ATTN: B. Zimmer

Lockheed Missiles & Space Co, Inc
ATTN: R. Sears
ATTN: J. Kumer

Lockheed Missiles & Space Co, Inc
ATTN: C. Old/Dept 68-21
ATTN: D. Churchill Dept 81-11
ATTN: Dept 60-12

M.I.T. Lincoln Lab
ATTN: D. Towle

MA COM Linkabit Inc
ATTN: H. Van Trees
ATTN: A. Viterbi
ATTN: I. Jacobs

Magnavox Govt & Indus Electronics Co
ATTN: G. White

Martin Marietta Corp
ATTN: R. Heffner

McDonnell Douglas Corp
ATTN: W. Olson
ATTN: Technical Library Services
ATTN: P. Halprin
ATTN: H. Spitzer

Meteor Communications Corp
ATTN: R. Leader

Mission Research Corp
ATTN: R. Hendrick
ATTN: C. Lauer
ATTN: R. Kilb
ATTN: F. Fajen
ATTN: R. Bigoni
ATTN: G. McCartor
ATTN: F. Guigliano
ATTN: Tech Library
ATTN: S. Gutsche
ATTN: R. Bogusch

DEPARTMENT OF DEFENSE CONTRACTORS (Continued)

Mitre Corp
ATTN: A. Kymmel
ATTN: B. Adams
ATTN: G. Harding
ATTN: C. Callahan
ATTN: MS J104 M. R. Oresp

Mitre Corp
ATTN: W. Hall
ATTN: M. Horrocks
ATTN: W. Foster
ATTN: J. Wheeler

Pacific-Sierra Research Corp
ATTN: E. Thomas
ATTN: E. Field, Jr
ATTN: H. Brode, Chairman SAGI

Pennsylvania State University
ATTN: Ionospheric Research Lab

Photometrics, Inc
ATTN: I. Kofsky

Physical Dynamics, Inc
ATTN: E. Fremouw

Physical Research, Inc
ATTN: R. Deliberis

R&D Associates
ATTN: R. Lelevier
ATTN: C. Greifinger
ATTN: R. Turco
ATTN: H. Ory
ATTN: W. Wright
ATTN: M. Gantsweg
ATTN: W. Karzas
ATTN: F. Gilmore

R&D Associates
ATTN: S. Yoon

Rand Corp
ATTN: E. Bedrozian
ATTN: C. Crain

Riverside Research Institute
ATTN: V. Trapani

Rockwell International Corp
ATTN: R. Buckner

Rockwell International Corp
ATTN: S. Gaillot

Santa Fe Corp
ATTN: D. Paolucci

DEPARTMENT OF DEFENSE CONTRACTORS (Continued)

Science Applications, Inc
ATTN: L. Linson
ATTN: C. Smith
ATTN: E. Straker
ATTN: D. Hamlin

Science Applications, Inc
ATTN: J. Cockayne

SRI International
ATTN: G. Price
ATTN: R. Tsunoda
ATTN: W. Chesnut
ATTN: R. Livingston
ATTN: D. Neilson
ATTN: J. Petrickes
ATTN: D. McDaniels
ATTN: M. Baron
ATTN: R. Leadabrand
ATTN: A. Burns
ATTN: C. Pino
ATTN: G. Smith
ATTN: V. Gonzales
ATTN: W. Jaye
ATTN: J. Vickrey

Stewart Radiance Laboratory
ATTN: J. Ulwick

Sylvania Systems Group
ATTN: R. Steinhoff

Sylvania Systems Group
ATTN: J. Concordia
ATTN: I. Kohlberg

Technology International Corp
ATTN: W. Boquist

Tri-Com, Inc
ATTN: D. Murray

TRW Electronics & Defense Sector
ATTN: G. Kirchner
ATTN: R. Plebuch
ATTN: D. Dee

Utah State University
ATTN: A. Steed
ATTN: D. Burt
ATTN: L. Jensen, Elec Eng Dept
ATTN: K. Baker, Dir Atmos & Space Sci

Visidyne, Inc
ATTN: C. Humphrey
ATTN: O. Shepard
ATTN: W. Reidy
ATTN: J. Carpenter

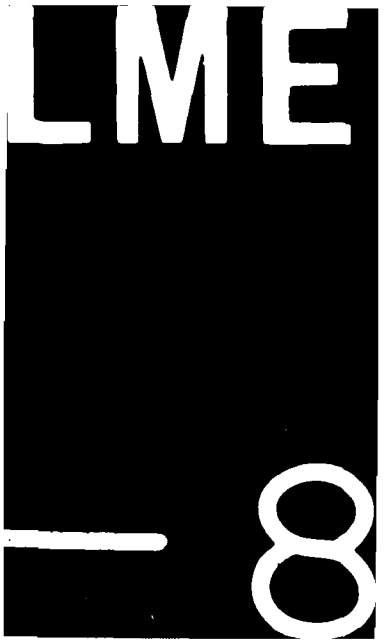
LME
8